Pulmonary blood flow evaluation using a dynamic flat-panel detector: Feasibility study with pulmonary diseases

doi: 10.1007/s11548-009-0364-4

Title

Pulmonary blood flow evaluation using a dynamic flat-panel detector: Feasibility study with pulmonary diseases

Authors * Corresponding author

Rie Tanaka, PhD[1]*, Shigeru Sanada, PhD[1], Masaki Fujimura, MD[2], Masahide Yasui, MD[2], Shiro Tsuji, MD[1], Norio Hayashi, PhD [3], Yuko Nanbu, CT[4], Osamu Matsui, MD[5]

Affiliation

[1] Department of Radiological Technology, Division of Health Sciences, Kanazawa University Graduate School of Medical Science; 5-11-80 Kodatsuno, Kanazawa, 920-0942, Japan

[2] Department of Cellular Transplantation Biology, Respiratory Tract Medicine, Kanazawa University Graduate School of Medical Science; 13-1 Takara-machi, Kanazawa, 920-8640, Japan

[3] Department of Radiology, Kanazawa University Hospital; 13-1 Takara-machi, Kanazawa, 920-8641, Japan

[4] Department of Clinical Laboratory, Kanazawa University Hospital; 13-1 Takara-machi, Kanazawa, 920-8641, Japan

[5] Department of Radiology, Kanazawa University Graduate School of Medical Science; 13-1 Takara-machi, Kanazawa, 920-8640, Japan

Telephone and Fax numbers and E-mail Address of Corresponding Author

Rie Tanaka, PhD

Tel: +81-76-265-2537

Fax: +81-76-234-4366

E-mail: rie44@mhs.mp.kanazawa-u.ac.jp

Kanazawa University Graduate School of Medical Science; 5-11-80 Kodatsuno, Kanazawa, 920-0942, Japan

Information concerning grants

This work was supported in part by a Grant-in-Aid for Scientific Research from the Japanese Ministry of Education, Culture, Sports, Science, and Technology, Konica Minolta Imaging Science Foundation, Suzuken Memorial Fuoudation, and Japan Science and Technology Agency.

Abstract

Purpose Pulmonary ventilation and circulation dynamics are reflected on fluoroscopic images as changes in X-ray translucency. The purpose of this study was to investigate the feasibility of non-contrast functional imaging using a dynamic flat-panel detector (FPD).

Methods Dynamic chest radiographs of 20 subjects (Abnormal, *n*=12; Normal, *n*=8) were obtained using the FPD system. Image analysis was performed to get qualitative perfusion mapping image; first, focal pixel value was defined. Second, lung area was determined and pulmonary hilar areas were eliminated. Third, one cardiac cycle was determined in each of the cases. Finally, total changes in pixel values during one cardiac cycle were calculated and their distributions were visualized with mapping on the original image. They were compared to the findings of lung perfusion scintigraphy.

Results In all normal controls, the total changes in pixel value in one cardiac cycle decreased from the hilar region to the peripheral region of the lung with left-right symmetric distribution. In contrast, in many abnormal cases, pulmonary blood flow disorder was indicated as a reduction of changes in pixel values on a mapping image. The findings of mapping image coincided with those of lung perfusion scintigraphy.

Conclusions Dynamic chest radiography using a FPD system with computer analysis is expected to be a new type of functional imaging which provides pulmonary blood flow distribution additionally.

Key words

Functional imaging; flat-panel detector; Pulmonary blood flow; Computer analysis; Chest radiography

Introduction

Dynamic flat-panel detectors (FPDs) allow acquisition of sequential chest radiographs with a large field of view and high image quality. While image intensifier systems are now being replaced with FPD systems, they are also expected to be useful as a new type of functional imaging system. Of particular note is blood flow evaluation based on changes in pixel values on dynamic chest radiographs without contrast media.

Pulmonary ventilation and circulation dynamics are reflected on fluoroscopic images as changes in X-ray translucency [1-4]. Thus, decreased airflow and blood flow should be indicated as a reduction of changes in pixel values. However, it is extremely difficult to evaluate blood flow patterns indicated as slight changes in X-ray translucency by visual observation. There have been many reports showing the feasibility of pulmonary densitometry [5-9]. These methods have not been adopted in clinical use because of technical limitations, such as poor image quality and a small field of view (FOV) [10].

At present, pulmonary blood flow is evaluated by lung perfusion scintigraphy, perfusion computed tomography (CT) [11-14], and magnetic resonance imaging (MRI) [15-19]. Although these examinations are useful for assessing the pulmonary blood flow pattern, they have certain disadvantages: In the CT approach the patients are exposed to a large exposure dose; the MRI approach takes cost and time. If pulmonary blood flow information becomes more readily available, it will be very helpful for determining an appropriate examination procedure and for patient follow-up.

Functional chest radiography using a dynamic FPD combined with computer analysis would overcome the difficulties encountered in these previous studies. We have developed computerized methods for evaluating pulmonary ventilation based on changes in pixel values both visually and quantitatively [20-22]. In a previous clinical study, areas with ventilation abnormality were indicated as areas of decreased changes in pixel values during respiration [23]. On the other hand, in a feasibility study of perfusion imaging using FPDs, it was demonstrated that pulmonary and cardiac blood flow were indicated as slight changes in pixel values on dynamic chest radiographs [24].

The purpose of this study was to develop a computerized method for evaluating pulmonary blood flow distribution and to assess the feasibility of newly-developed method in comparison with the findings of lung perfusion scintigraphy.

Materials and methods

Study population

Approval for the study was obtained from our institutional review board, and the

subjects gave written informed consent prior to participation. Dynamic chest radiographs of 20 subjects (Abnormal, *n*=12; Normal, *n*=8) were obtained in this study. The abnormal subjects (39–82 years old; mean, 67 years old; M:F=9:3) had been diagnosed with pulmonary diseases, such as chronic obstructive pulmonary disease (COPD), asthma, bronchiolitis obliterans, atelectasis, and interstitial pulmonary fibrosis, based on findings on CT, pulmonary functional tests (PFT), and other clinical findings. In addition, pulmonary blood flow disorder was diagnosed by lung perfusion scintigraphy. The normal controls (21–51 years old; mean, 26 years old; M:F=7:1) had no underlying asthma or smoking history, and they were confirmed to be normal based on their chest radiographs and the results of PFT.

Image acquisition

Dynamic chest radiographs were obtained using an FPD system (SONIAL VISION Safire II; Shimadzu, Kyoto, Japan). Thirty images were obtained in 4 s with exposure under the following conditions: 110 kV, 80 mA, 6.3 ms, source to image distance 1.5 m, 7.5 frames per second (fps). Imaging was performed in the standing position, posteroanterior direction, and rest expiratory level of breath-holding, which was the most stable respiratory phase for patients. Total exposure dose was approximately 0.6 mGy, which was less than that in lateral chest radiography determined as the guidance level of the International Atomic Energy Agency (IAEA) (1.5 mGy) [25]. The matrix size was 1440×1440 pixels, the pixel size was 260×260 μm, FOV was 38×38 cm, and the grayscale range of the images was 16 bits, which was proportional to the incident exposure in the FPD.

Image analysis

Image analysis was performed on a personal computer (CPU, Pentium 4, 2.6 GHz; Memory, 2 GB; operating system, Windows XP; Microsoft, Redmond, WA) with our algorithm (Development environment, C++Builder; Borland, Scotts Valley, CA), to quantify and visualize slight changes in pixel values in lung area. The total time required for image analysis, from image input to output of the results, was a few seconds plus a few minutes for preprocessing purposes.

Image analysis was performed to get qualitative perfusion mapping image; first, focal pixel value was defined. Second, lung area was determined and pulmonary hilar areas were eliminated. Third, one cardiac cycle was determined in each of the cases. Finally, average score of the focal pixel value and summation of absolute values in a single cardiac phase was calculated, and distribution of the summation in whole

lung area was visualized.

To facilitate image analysis, images were reduced to 12 bits. Low pixel values were related to dark areas in the images, and these in turn were related to high X-ray translucency in this study. The lung area was determined by edge detection using the first derivative technique and iterative contour-smoothing algorithm [26,27]. The hilar regions were excluded from the lung area manually, which took a few minutes per case. For determination of cardiac phase, average pixel value was measured in a region of interest (ROI) located just outside of the left ventricular wall throughout all frames [29]. After these preprocessing steps, increase in pixel values was determined as the diastole phase and decrease in pixel values as the systole phase. The frames composing a whole cardiac phase were determined and the first complete cycle was selected for the following procedures.

The images were divided into 64×64 blocks 20 pixels (=6 mm) on a side, and the average pixel value in each block $P_n(x, y)$ was calculated, as shown in Fig. 1. Here, x and y are the coordinates of blocks in the horizontal and vertical directions, respectively, and n is the frame number. The reason for providing the average pixel value by block unit is to reduce the influence of movement, dilation, contraction of vessels, and image noise. The block size was the smallest determined experimentally in which defects in the blood flow could be detected by the present method under ideal conditions without the influence of the ribs [24]. Fluctuation was found in adjacent frames in $P_n(x, y)$ due to X-ray output and image noise, which was only about 0.04% of the total grayscale. Thus, it was eliminated by smoothing pixel values, averaging adjacent values, in the time axis direction, as shown in Fig. 1.

$P_{ave}(x, y)$, the average pixel value of $P_n(x, y)$ in one cardiac cycle, was then calculated, and the differences between $P_n(x, y)$ and $P_{ave}(x, y)$ were determined throughout one cardiac cycle in each block. The sum of the absolute differences was finally output as $P_{total}(x, y)$, representing the total changes in pixel values in each block in one cardiac cycle, assuming that it reflects the amount of input–output blood flow in the local lung area in one cardiac cycle. $P_{ave}(x, y)$ and $P_{total}(x, y)$ are defined as follows;

$$P_{ave}(x, y) = [P_0(x, y) + P_1(x, y) + ... + P_n(x, y)]/N \quad (0 < n < N)$$

$$P_{total}(x, y) = \sum | P_n(x, y) - P_{ave}(x, y) | \quad (0 < n < N)$$

where N is the number of frames composed of one cardiac cycle.

To facilitate visual evaluation, $P_{total}(x, y)$, which is the total change in pixel value in one cardiac cycle, was mapped on the original image using a grayscale in which small changes were shown in black and large changes were shown in white (hereafter

called “perfusion mapping image”). The result images were compared to the findings of lung perfusion scintigraphy.

Comparison with findings in lung perfusion scintigraphy

To investigate the clinical usefulness of the present method, perfusion mapping images were compared with the findings of lung perfusion scintigraphy. A specialist in nuclear medicine evaluated the lung perfusion scintigrams and classified lung area into three classes, *i.e.*, perfusion defect, reduced blood flow, or normal area. The perfusion defect and reduced blood flow areas were traced in solid and broken lines, respectively.

Results

In all normal controls, the total changes in pixel values in one cardiac cycle, $P_{total}(x, y)$, decreased from the hilar region to the peripheral region of the lung with a left-right symmetric distribution as shown in Fig. 2 (22-year-old man). In contrast, many abnormal cases showed a nonuniform distribution on perfusion mapping images, which were different from the normal pattern, as shown in Figs. 3–5.

Figure 3 shows the results in a patient with pulmonary fibrosis (82-year-old man). Perfusion scintigraphy showed marked reduction in blood flow in the left lung in comparison with the right lung. The perfusion mapping image also showed reduced total changes in pixel values over the left lung. Figure 4 shows the results in a patient with pleuropulmonary diseases (74-year-old man). This patient had reduced blood flow area in the right whole lung, and left upper and lower lung as shown in Fig. 4b. The area appeared white in the perfusion mapping image, indicating no or reduced changes in pixel values on dynamic chest radiographs.

In two cases, blood flow distribution was not consistent with the distribution of changes in pixel values. Figure 5 shows the results in a patient with pulmonary fibrosis (56-year-old woman). Perfusion scintigraphy showed that there were no or reduced blood flow areas in the upper regions of both lungs. These areas showed reduced changes in pixel values in the perfusion mapping image. However, the remaining area also had reduced changes in pixel values as shown by the arrows in Fig. 5.

DISCUSSION

In the normal controls, perfusion mapping images showed that the distribution of changes in pixel values was consistent with normal pulmonary blood flow distribution, which decreases from the hilar region to the peripheral regions gradually and symmetrically [29,30]. Furthermore, in most of the abnormal cases, the distribution of

changes in pixel values was consistent with the findings of lung perfusion scintigraphy. These results indicated that pulmonary blood flow could be evaluated based on changes in pixel values.

However, in two cases, the results using the present method were different from those of lung perfusion scintigraphy. The false positive was thought to be due to differences in the items measured; lung perfusion scintigraphy measures nuclear radiation from radiolabeled compound, *e.g.*, ^{99m}Tc-MAA, which is trapped in the capillary and reflects distribution of the pulmonary artery blood flow, while the present method measures changes in pixel values, *i.e.*, X-ray translucency, in the lung area on dynamic chest radiographs, assuming that they reflect changes in blood volume. In addition, "mismatch" may be caused by differences in body posture during imaging and patient's condition. Further studies in clinical cases are required to address these points.

The present method has advantages in that it takes less time for imaging and analysis, has an acceptable total patient dose, and has costs comparable to those of conventional chest radiography except for the cost of system installation. Although the present method lacks 3D anatomic information, it can be used as a rapid substitute for lung perfusion scintigraphy, perfusion CT, and MRI in clinical follow-up and therapy evaluation. The image analysis method could be applied to dynamic CT as an optional means of evaluating blood flow. It would be advantageous for patients to be provided additional functional information in routine radiographic studies.

Some limitations should be noted. The dilation and constriction of pulmonary vessels and their movements are also included in the changes in pixel values. Furthermore, the changes in pixel values do not show the absolute blood volume. However, the results indicated that perfusion mapping image could provide relative measure related to pulmonary perfusion. Thus, the present method would be utilized as a means to evaluate pulmonary blood distribution in each patient rather than inter-subject comparison. For practical use, it is necessary to establish diagnosis criteria, particularly to address the diagnostic ability for pulmonary embolism. In addition, to ensure the maximum diagnostic performance of this method, it is also necessary to optimize the imaging conditions, block size for the measurement of pixel value, and cardiac phase to be analyzed.

In conclusion, pulmonary blood flow distribution could be evaluated by functional chest radiography using a dynamic FPD system combined with real-time computer analysis. Pulmonary blood flow disorder was indicated as a reduction of changes in pixel values. The present method is a rapid, simple, and non-invasive

method for evaluating pulmonary circulation, and will be useful as an additional examination in chest radiography.

Acknowledgment

The authors are grateful to Naoki Kikuchi and Atsushi Kameoka at Marubun Tsusho Co., LTD, and Takeshi Matsui, Masaaki Kawamura, Tomoyuki Yamamoto, and the technologists of the Dept. of Radiology, Kanazawa University Hospital, who assisted with data acquisition. The authors thank the editors and reviewers who spent a great deal of time and gave us informative advice for improving our manuscript.

References

1. Heyneman LE (2005) The chest radiograph : Reflections on cardiac physiology. Radiological Society of North America. Scientific Assembly and Annual Meeting Program 2005; pp 145
2. Felson B (1973) Chest roentgenology. Philadelphia, London, Toronto
3. Goodman LR (2006) Felson's Principles of Chest Roentgenology. A programmed text, 3rd ed. Philadelphia, London, Toronto
4. Squire LF, Novelline RA (1972) Fundamentals of Radiology, 4th ed. Cambridge, Massachusetts, and London.
5. Silverman NR (1972) Clinical video-densitometry. Pulmonary ventilation analysis. Radiology 103:263-265
6. Silverman NR, Intaglietta M, Simon AL, et al (1972) Determination of pulmonary pulsatile perfusion by fluoroscopic videodensitometry. J Appl Physiol 33:147-149
7. Silverman NR, Intaglietta M, and Tompkins WR. (1973) Pulmonary ventilation and perfusion during graded pulmonary arterial occlusion. J Appl Physiol 34:726-731
8. Bursch JH (1985) Densitometric studies in digital subtraction angiography: assessment of pulmonary and myocardial perfusion. Herz 10:208-214
9. Liang J, Jarvi T, Kiuru A, et al (2003) Dynamic chest image analysis: model-based perfusion analysis in dynamic pulmonary imaging. J Applied Signal Process 5:437-448
10. Fujita H, Doi K, MacMahon H, et al (1987) Basic imaging properties of a large image intensifier-TV digital chest radiographic system. Invest Radiol 22:328-335
11. Groell R, Peichel KH, Uggowitzer MM, et al (1999) Computed tomography densitometry of the lung: a method to assess perfusion defects in acute pulmonary embolism. Eur J Radiol 32:192-196
12. Herzog P, Wildberger JE, Niethammer M, et al (2003) CT perfusion imaging of the lung in pulmonary embolism. Acad Radiol 10:1132-1146
13. Wildberger JE, Schoepf UJ, Mahnken AH, et al (2005) Approaches to CT perfusion imaging in pulmonary embolism. Semin Roentgenol 40:64-73.
14. Easley RB, Fuld MK, Fernandez-Bustamante A, et al (2006) Mechanism of hypoxemia in acute lung injury evaluated by multidetector-row CT. Acad Radiol 13: 916-921
15. Carr JC, Laub G, Zheng J, et al (2002) Time-resolved three-dimensional pulmonary MR angiography and perfusion imaging with ultrashort repetition time. Acad Radiol 9:1407-1418
16. Gee J, Sundaram T, Hasegawa I, et al (2003) Characterization of regional pulmonary mechanics from serial magnetic resonance imaging data. Acad Radiol 10:

1147-1152
17. Hong C, Leawoods JC, Yablonskiy DA, et al (2005) Feasibility of combining MR perfusion, angiography, and 3He ventilation imaging for evaluation of lung function in a porcine model. Acad Radiol 12: 202-209
18. Molinari F, Fink C, Risse F, et al (2006) Assessment of differential pulmonary blood flow using perfusion magnetic resonance imaging: comparison with radionuclide perfusion scintigraphy. Invest Radiol 41:624-630
19. Bolar DS, Levin DL, Hopkins SR, et al (2006) Quantification of regional pulmonary blood flow using ASL-FAIRER. Magn Reson Med 55:1308-1317
20. Tanaka R, Sanada S, Kobayashi T, et al (2006) Computerized methods for determining respiratory phase on dynamic chest radiographs obtained by a dynamic flat-panel detector (FPD) system. J Digit Imaging 19:41-51
21. Tanaka R, Sanada S, Suzuki M, et al (2004) Breathing chest radiography using a dynamic flat-panel detector combined with computer analysis. Med Phys 31:2254-2262.
22. Tanaka R, Sanada S, Okazaki N, et al (2008) Detectability of regional lung ventilation with flat-panel detector-based dynamic radiography. J Digit Imaging 21:109-120
23. Tanaka R, Sanada S, Okazaki N, et al (2006) Evaluation of pulmonary function using breathing chest radiography with a dynamic flat panel detector: primary results in pulmonary diseases. Invest Radiol 41:735-745
24. Tanaka R, Sanada S, Okazaki N, et al (2008) Development of functional chest imaging with a dynamic flat-panel detector (FPD). Radiological physics and technology 1: 137-143
25. International basic safety standards for protection aginst ionizing radiation and for the safety of radiation sources (1996) Vienna:International atomic energy agency (IAEA)
26. Xu XW, Doi K (1995) Image feature analysis for computer-aided diagnosis: accurate determination of ribcage boundary in chest radiographs. Med Phys 22:617-626
27. Li L, Zheng Y, Kallergi M, et al (2001) Improved method for automatic identification of lung regions on chest radiographs. Acad Radiol 8:629-638
28. Myers PH, Nice CM, Becker HC, et al (1964) Automated computer analysis of radiographic images, Radiology 83:1029-1033.
29. Hansen JT and Koeppen BM (2002) Cardiovascular Physiology, In: Netter's Atlas of Human Physiology (Netter Basic Science). Teterboro, New Jersey
30. Rees D (2002) Essential Statistics, 4th ed. (Text in statistical science) Florida

Figures captions

Fig. 1 Process for quantifying changes in pixel values. (a) One frame divided into 64×64 blocks and enlarged view of a block. (b) Average pixel value measured during one cardiac cycle in a block. The broken and solid lines are unprocessed and smoothed $P_n(x, y)$, respectively. The horizontal broken line and bar graphs are $P_{ave}(x, y)$ and the differences between $P_{ave}(x, y)$ and $P_n(x, y)$, respectively. The dotted line is the final output, $P_{total}(x, y)$.

Fig. 2 Results in a normal control subject (22-year-old man). (a) One frame of dynamic chest radiograph. (b) Perfusion mapping image. Total changes in pixel values in one cardiac cycle decreased from the hilar region to the peripheral region of the lung with a symmetric distribution.

Fig. 3 Results in a patient with pulmonary fibrosis (82-year-old man). (a) One frame of dynamic chest radiograph. (b) Lung perfusion scintigram (99mTc-MAA). The area surrounded by a broken line shows reduced blood flow. (c) Perfusion mapping image. The area of reduced blood flow is indicated as reduced changes in pixel values. (d) Computed tomography (CT) (coronal section). (e)-(g) CT (Axial section).

Fig. 4 Results in a patient with pleuropulmonary disease (74-year-old man). (a) One frame of dynamic chest radiograph. (b) Lung perfusion scintigram (99mTc-MAA). The area surrounded by a broken line shows reduced blood flow. (c) Perfusion mapping image. The area of reduced blood flow is indicated as reduced changes in pixel values. (d) Computed tomography (CT) (coronal section). (e)-(g) CT (Axial section).

Fig. 5 Results in a patient with pulmonary fibrosis (56-year-old woman). (a) One frame of dynamic chest radiograph. (b) Lung perfusion scintigram (99mTc-MAA). The area surrounded by solid and broken lines show defective and reduced blood flow respectively. (c) Perfusion mapping image. The areas of reduced blood flow areas in the upper regions of both lungs are indicated as areas with reduced changes in pixel values. However, the remaining area in the left middle lung also showed reduced changes in pixel values, as indicated by the arrows. (d) Computed tomography (CT) (coronal section). (e)-(g) CT (Axial section).

Figure 1

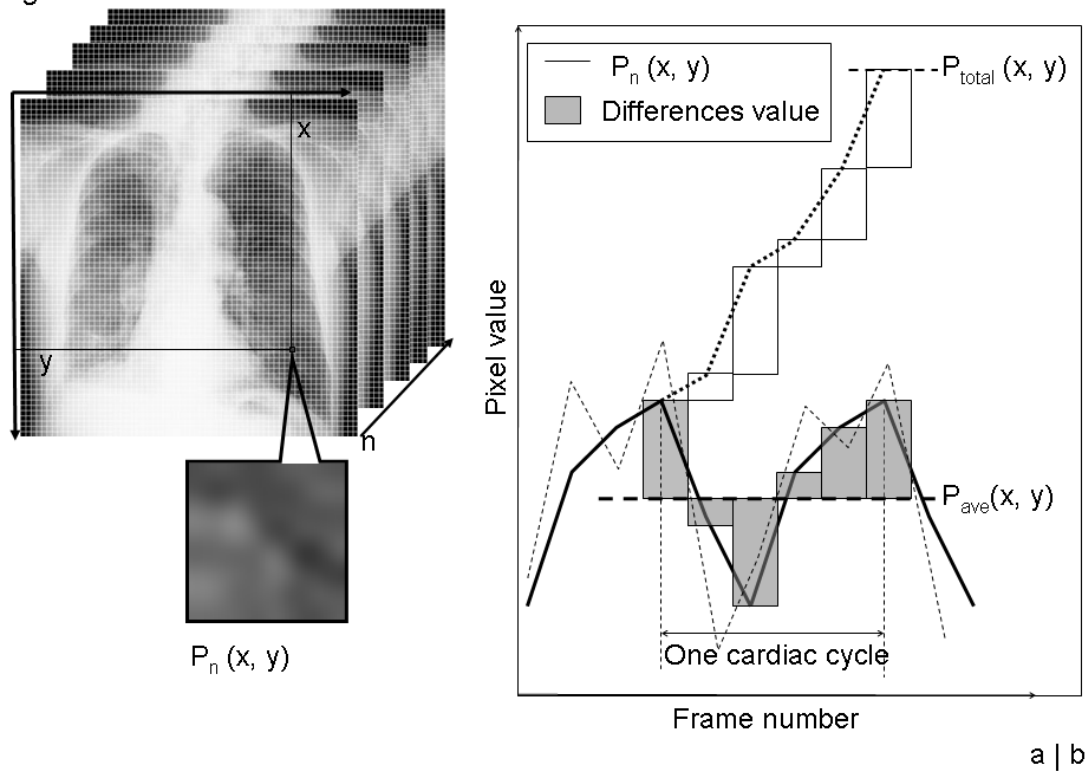

Fig. 1 Process for quantifying changes in pixel value. (a) One frame divided into 64×64 blocks and enlarged view of a block. (b) Average pixel value measured during one cardiac cycle in a block. The broken and solid lines are unprocessed and smoothed $P_n(x, y)$, respectively. The horizontal broken line and bar graphs are $P_{ave}(x, y)$ and the differences between $P_{ave}(x, y)$ and $P_n(x, y)$, respectively. The dotted line is the final output, $P_{total}(x, y)$.

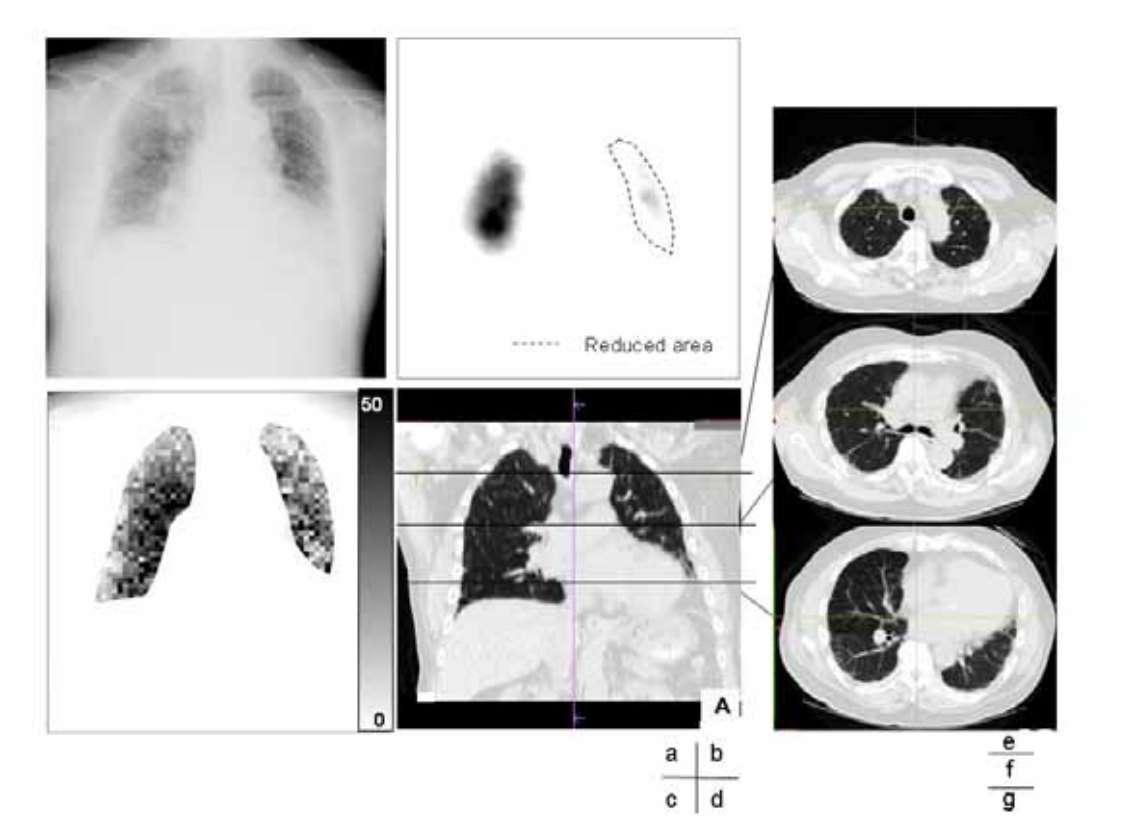

Fig. 2 Results in a normal control subject (22-year-old man). (a) One frame of dynamic chest radiograph. (b) Perfusion mapping image. Total changes in pixel values in one cardiac cycle decreased from the hilar region to the peripheral region of the lung with a symmetric distribution.

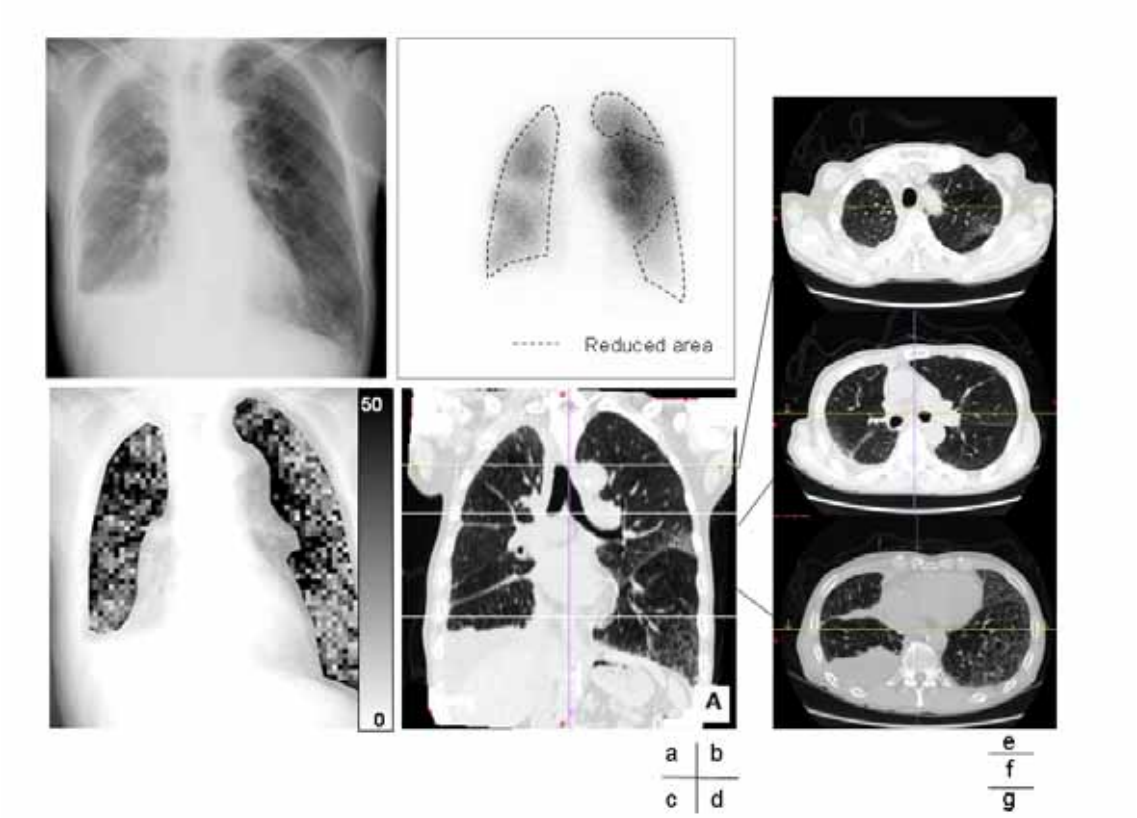

Fig. 3 Results in a patient with pulmonary fibrosis (82-year-old man). (a) One frame of dynamic chest radiograph. (b) Lung perfusion scintigram (99mTc-MAA). The area surrounded by a broken line shows reduced blood flow. (c) Perfusion mapping image. The area of reduced blood flow is indicated as reduced changes in pixel values. (d) Computed tomography (CT) (coronal section). (e)-(g) CT (Axial section).

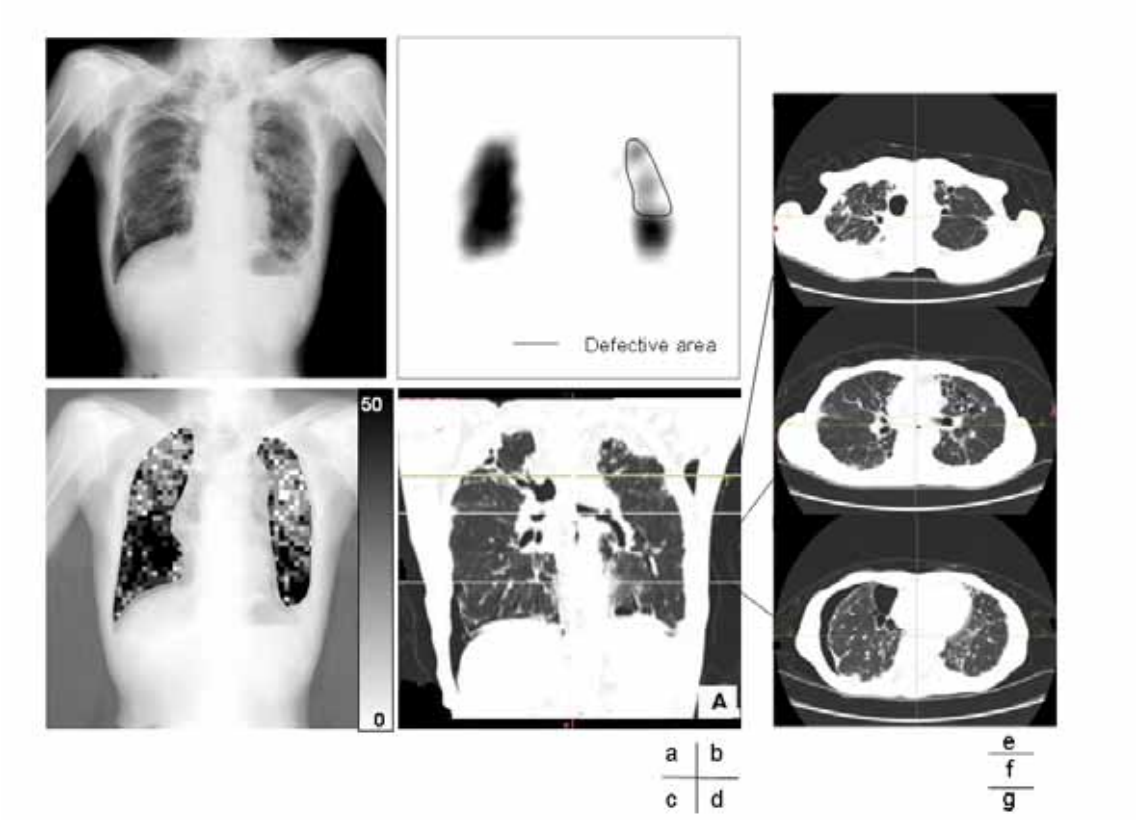

Fig. 4 Results in a patient with pleuropulmonary disease (74-year-old man). (a) One frame of dynamic chest radiograph. (b) Lung perfusion scintigram (99mTc-MAA). The area surrounded by a broken line shows reduced blood flow. (c) Perfusion mapping image. The area of reduced blood flow is indicated as reduced changes in pixel values. (d) Computed tomography (CT) (coronal section). (e)-(g) CT (Axial section).

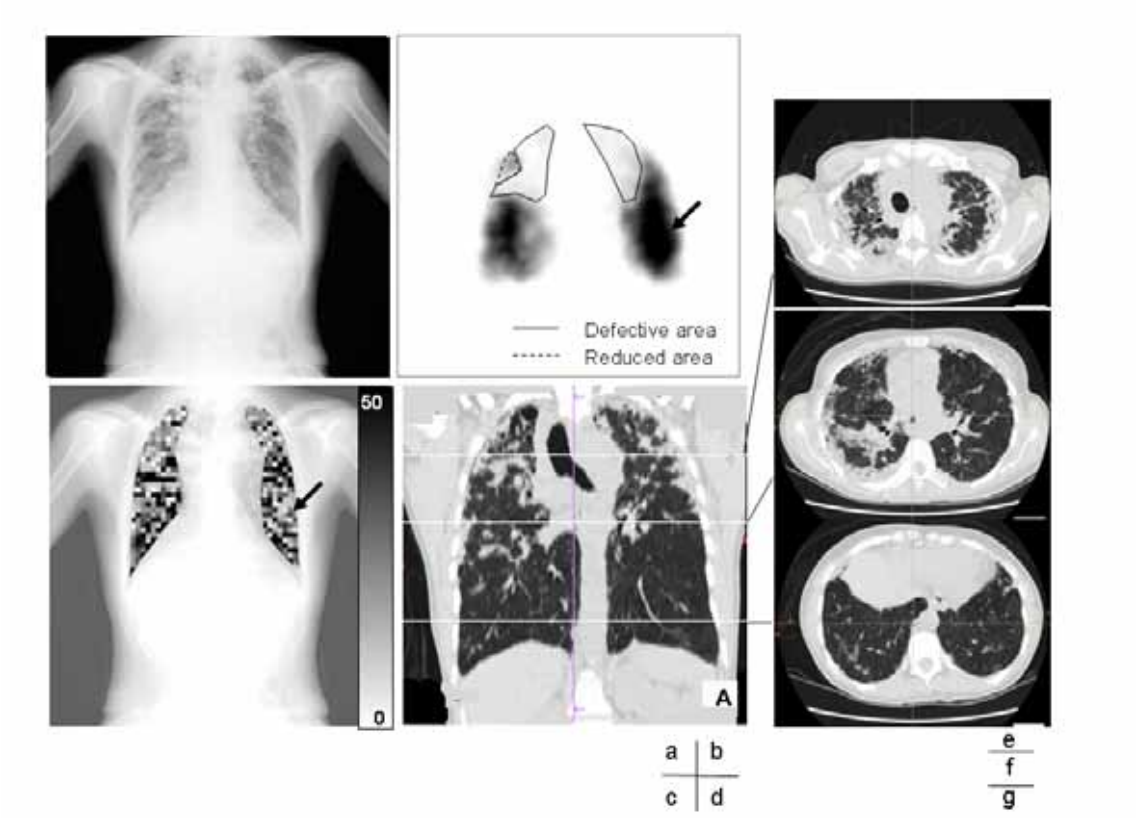

Fig. 5 Results in a patient with pulmonary fibrosis (56-year-old woman). (a) One frame of dynamic chest radiograph. (b) Lung perfusion scintigram (99mTc-MAA). The area surrounded by solid and broken lines show defective and reduced blood flow respectively. (c) Perfusion mapping image. The areas of reduced blood flow areas in the upper regions of both lungs are indicated as areas with reduced changes in pixel values. However, the remaining area in the left middle lung also showed reduced changes in pixel values, as indicated by the arrows. (d) Computed tomography (CT) (coronal section). (e)-(g) CT (Axial section).